PCCP

Physical Chemistry Chemical Physics

rsc.li/pccp

POOL RULES (VCD EDITION)

Follow these rules for optimal spectral results

- Shower Before Measurement
- No Precipitation Allowed
- No Unassigned Peaks
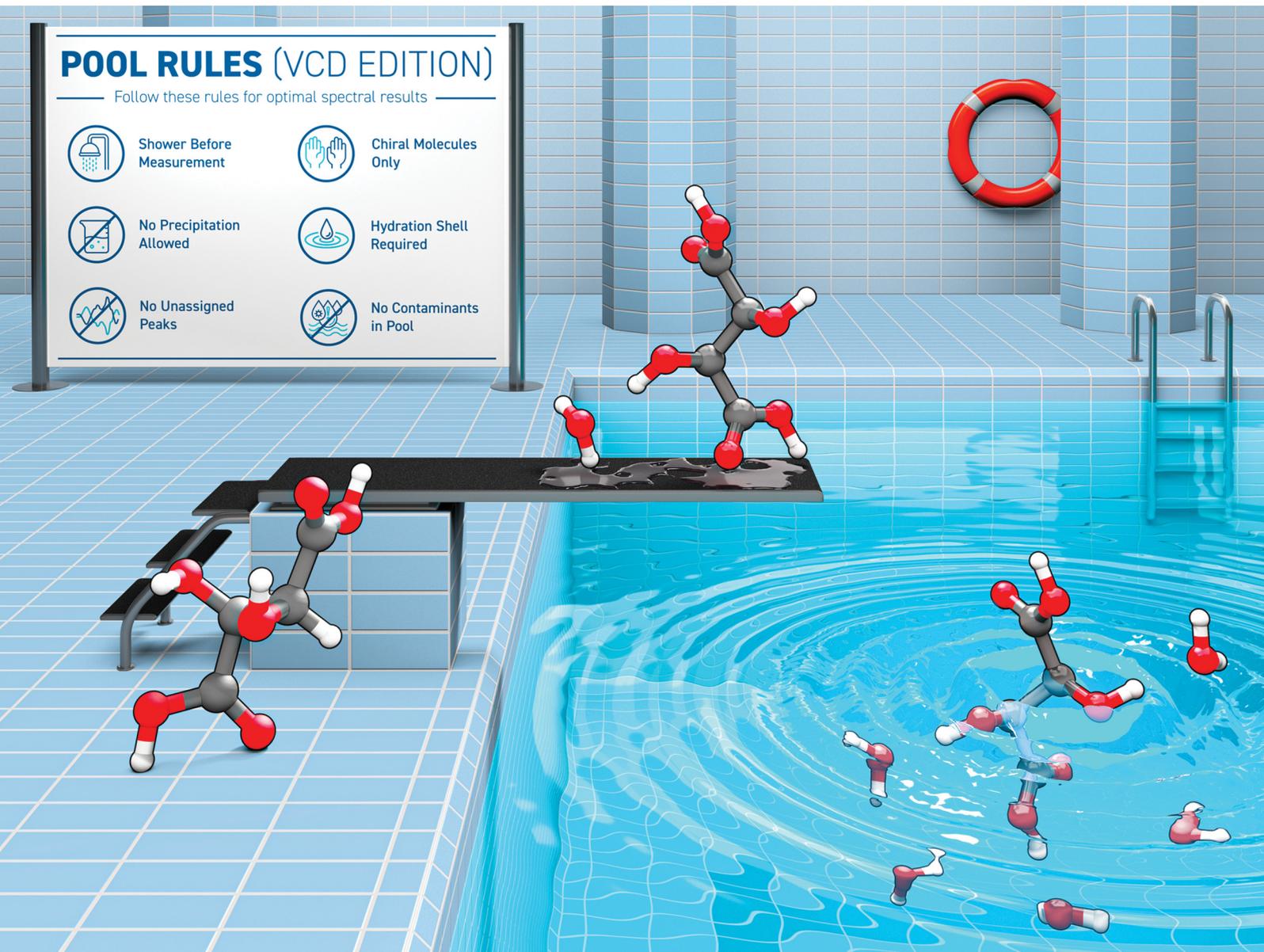- Chiral Molecules Only
- Hydration Shell Required
- No Contaminants in Pool

ROYAL SOCIETY
OF **CHEMISTRY**

PAPER
Deborah A. Drost and Christian Merten
Vibrational circular dichroism of tartaric acid in water

PCCP
Owner Societies

Check for updates

Vibrational circular dichroism of tartaric acid in water

Deborah A. Drost [ID] and Christian Merten [ID] *

Although tartaric acid (**TA**) and its esters have been among the first molecules to be characterized by means of VCD spectroscopy, the experimental spectra of **TA** recorded in water have not yet been reproduced using DFT-based spectral calculations. In the present study, we investigated the VCD spectra of **TA** in water and heavy water. We demonstrate that the commonly applied micro-solvation approach, *i.e.*, the modelling of the effect of solvation by considering only a few solute–solvent interactions, is not sufficient to reproduce the experimentally observed VCD signatures. Following a recently introduced solvent-shell approach, we thus simulated the spectra based on the clusters of 30 water molecules (∼1.5 solvation shell), which were extracted from QM/MM molecular dynamics simulations at the AM1 and PM6 levels for the solute. An exceptionally good match with the experiment is achieved for both **TA**–$(H_2O)_{30}$ and **TA**-d_4–$(D_2O)_{30}$, which stressed the need to consider a significant number of solvent molecules in the spectral prediction. The same approach was applied to disodium tartrate (**TA^{2-}**), for which the QM/MM MD simulations surprisingly revealed different conformational preferences depending on the chosen semi-empirical level. By comparison of the simulated VCD spectra obtained for the two conformational distributions, it is confirmed that the AM1-based MD simulations provide a better microscopic picture of **TA^{2-}** in water.

Introduction

Vibrational circular dichroism (VCD) spectroscopy is a powerful tool for the characterization of chiral molecules.[1,2] Comparing experimental and computed spectra enables the determination of conformational preferences and absolute configurations (ACs) of chiral solutes.[3–5] VCD spectra were demonstrated to be very sensitive to intermolecular interactions,[6] and were utilized in studies on supramolecular structures[7–15] and asymmetric catalysts.[16–20] Furthermore, due to its sensitivity to conformational changes, VCD spectroscopy can be used to characterize solute–solvent interactions.[21–28]

Despite the obvious interest in using VCD spectroscopy to characterize chiral molecules in aqueous solutions,[29,30] it imposes both experimental and computational challenges. Firstly, water is a strong IR absorber, so that short optical pathlengths below 8 μm and quite high concentrations in the molar range are required. This limits its applicability, as solubilities are often not sufficiently high. Secondly, the computational analysis requires the modelling of explicit solute–solvent interactions with water. While only a few water molecules were occasionally considered sufficient to reproduce the

experimental signatures,[31–34] we recently found that the relative orientation of single water molecules in clusters of zwitterionic proline with five water molecules strongly alters the computed VCD band shapes.[35] These changes could be traced back to vibrational modes of proline, which coupled to modes of water. We thus established a computational workflow to compute the VCD/IR spectra of aqueous solutions by considering large solute–solvent clusters. In particular, we carried out molecular dynamics (MD) simulations to sample the conformational spaces of the solute and solvent and simulated the spectra of proline in various protonation states based on clusters with 30 water molecules. This method, which is referred to as the solvent shell approach in extension of the term microsolvation, demonstrated very good agreement with the experimental spectra.

Tartaric acid (**TA**) and its esters were used as early model systems for the interpretation of VCD spectra based on various theoretical models. Moscowitz *et al.* were the first to report the VCD spectra in the C–H stretching region of **TA**-d_4 in D_2O,[36] while Keiderling first reported the VCD spectra of dimethyl tartrate in the OH/CH and C=O stretching regions.[37,38] Both used a coupled oscillator model for spectral interpretations. Polavarapu *et al.* later investigated **TA** and its esters in DMSO, CCl_4, $CDCl_3$ and CS_2 below 1600 cm^{-1}, and interpreted the spectra using the charge flow model for VCD.[39] The experimental VCD of the disodium salt in D_2O was reported by Brizard *et al.*, but no complementary spectral calculations were

Ruhr-Universität Bochum, Fakultät für Chemie und Biochemie, Organische Chemie II, Universitätsstraße 150, 44801 Bochum, Germany.
E-mail: christian.merten@ruhr-uni-bochum.de; Web: https://www.mertenlab.de

This journal is © the Owner Societies 2026

Phys. Chem. Chem. Phys., 2026, **28**, 1111–1117 | 1111

carried out.[40] More recently, Polavarapu *et al.* revisited the spectra of **TA** in DMSO to evaluate the quantum cluster growth method to generate micro-solvated clusters.[41] For completeness, it should be mentioned that the experimental Raman optical activity spectra of **TA** in H_2O and D_2O were reported by Barron *et al.*[42] The ROA study was complemented with spectral predictions on the isolated molecule and without considering the influence of the solvent.

Interestingly, to the best of our knowledge, there is no computational study aiming to fully simulate the VCD spectra of **TA** or the tartrate dianion (**TA^{2-}**) in H_2O or D_2O. Herein, we thus strive to compare the micro-solvation and the solvent-shell approach for spectral calculations. It will be demonstrated that the prediction requires a considerable number of water molecules. Furthermore, we will highlight that the VCD spectra can be used to differentiate conformational distributions predicted by QM/MM-MD simulations at different semi-empirical levels of theory.

Experimental and computational details

Materials

Both enantiomers were obtained from commercial sources (Sigma Aldrich) and used without further purification.

IR and VCD spectroscopy

The IR and VCD spectra were recorded on a Bruker Vertex FT-IR spectrometer equipped with a PMA 50 module for VCD measurements. Samples were held in a transmission cell assembled from a CaF_2 window with a central 6 μm deep pit, which ensures a constant path length, and a flat BaF_2 or CaF_2 window as a counter-window. The cell was held at a constant temperature of 22 °C. To avoid artefacts caused by total absorbance, concentrations were adjusted so that the IR spectra did not exceed an absorbance of 0.9 in the region of interest. Spectra were recorded at room temperature with a spectral resolution of 4 cm^{-1} by accumulating 32 scans for the IR and $\sim$32 000 scans (8 hours accumulation time) for VCD. Baseline correction of the VCD spectra was initially done by subtraction of the spectra of the racemic mixture recorded under identical conditions. While this procedure gave reasonably good mirror-image spectra (*cf.* Fig. S1), the spectra presented in the main text are baseline corrected by subtracting the half-sum spectrum of the enantiomers, that is, the average of the VCD spectra recorded for L- and D-tartaric acid.

Computational details

The MD simulations have been carried out using the Amber22 Molecular Dynamics Software Package.[43] Input files were prepared and trajectories were evaluated using AmberTools23. QM/MM MD simulations were run using AM1 or PM6 for the solute and 510–560 TIP3P water molecules around it. Following the usual equilibration steps, NpT simulations were run for a simulation time of 30 ns. Four independent trajectories were

simulated from different starting structures and the convergence of the conformational distribution was evaluated by comparison of characteristic dihedral angle distributions. From each trajectory, snapshots were extracted for every 30 ps and structures were reduced to contain the closest 30 water molecules, which accounts for $\sim$1.5 solvation shells. This number of solvent molecules was considered a reasonable compromise between considering only one solvent shell, which bares the risk of too strong rearrangement of the solvent structure during optimization, and full two solvent shells that require significantly more sampling. These reduced snapshots were subjected to geometry optimizations and frequency calculations at the B3LYP(G)/def2-TZVP/CPCM(water) level of theory using the ORCA6 software package.[44–46] For calculations in D_2O, all acidic hydrogen atoms were substituted with deuterium and spectral calculations were repeated at the same level of theory. The spectra were simulated by assigning Lorentzian band shapes with a half-width at half-height (HWHH) of 6 cm^{-1} to the computed IR and VCD intensities. The calculated VCD spectra were multiplied by a factor of 2 or 3 for a better comparison with the experimental spectra. The narrower HWHH resulted in less smooth but overall more intense spectra that required less scaling in intensities. Hence, the smoother spectra were preferred for comparison with the broad experimental band shapes. A frequency scaling factor of 0.99 was applied.

For the analysis of the MD trajectories, the first and second solvation shells were defined within 3.4 Å and 5.0 Å following the default settings of the watershell command of the CPPTRAJ program provided with AmberTools23. Likewise, intra- and intermolecular hydrogen bonds were counted when contacts between the heavy atom of the donor and the acceptor were shorter than 3.4 Å using the hbond command. After the geometry optimizations at the DFT level, the hydrogen bonds have been evaluated using a distance cutoff of 2 Å between the donor hydrogen and the acceptor O atom and X–H$\cdots$O angles between 120° and 180°.

Results and discussion

Experimental spectra of TA at different pH values

Dissolving **TA** at 1.5 M in distilled water resulted in samples with a pH of 1.5, corresponding to a dissociation of only $\sim$2.5% of the **TA** molecules ($pK_{a1} \approx 2.65$).[47] Likewise, a 1.5 M solution of **TA** in 4 M NaOH gave samples with a pH of 13.5, corresponding to complete dissociation (**TA^{2-}**). The IR and VCD spectra of both enantiomers and the racemic mixture of **TA** were recorded under these pH conditions (Fig. 1 and Fig. S1). Notably, water exhibits a broad absorption band around 1645 cm^{-1} due to the water bending modes, and the water libration modes can be identified as an onset of a band below 1050 cm^{-1}. Due to total absorbance, the strong bands in the region above 1500 cm^{-1} limit VCD measurements to the frequency range between 1500 and 1050 cm^{-1}. Nevertheless, a characteristic change in the C=O stretching band from
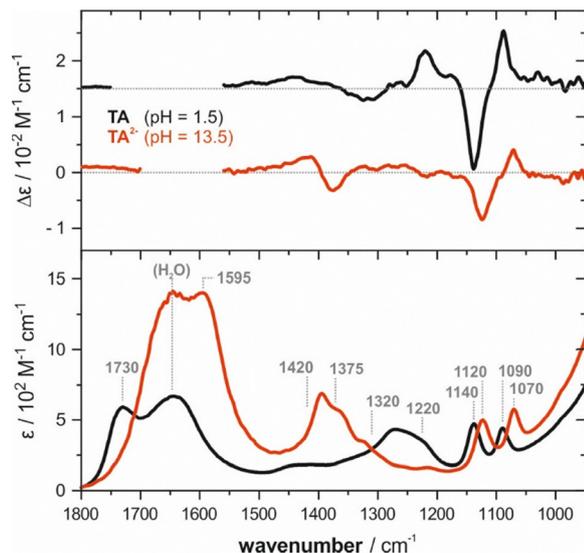
1112 | *Phys. Chem. Chem. Phys.*, 2026, **28**, 1111–1117

This journal is © the Owner Societies 2026

Fig. 1 VCD and IR spectra of 1.5 M solution of tartaric acid at pH 1.5 and 13.5 recorded at a 6 μm path length.

1730 cm^{-1} (**TA**) to 1595 cm^{-1} (**TA^{2-}**) can still be noted in the IR spectra. Further distinct changes are found for the broad bands between 1300 and 1200 cm^{-1} in the spectrum of **TA**, which shift to $1400–1300 \text{ cm}^{-1}$ for **TA^{2-}**. Likewise, the two distinct bands at $1140/1090 \text{ cm}^{-1}$ of **TA** show a red-shift towards $1120/1070 \text{ cm}^{-1}$ upon deprotonation. In the VCD spectra, the change in the protonation state results not only in band shifts but also in distinct changes in the band patterns. While the (−/+)-pattern of the bands around 1100 cm^{-1} only experiences the corresponding shifts in frequency seen already in the IR region, the (+/−)-couplet in the range of $1400–1300 \text{ cm}^{-1}$ sharpens upon deprotonation and the broad structured bands in the spectrum of **TA** vanish.

Neutral tartaric acid in H₂O

The conformational space of **TA** is defined by seven torsional angles (Fig. 2). For our analysis of the spectra of **TA** in H₂O, we assumed (and later confirmed by MD simulations) that the carboxylic acid groups remain in the *cis*-conformation ($\delta \approx 0$), as this is the commonly found structure in the solution phase.[21,48] Notably, in a rotational spectroscopy study, the vicinity to hydroxy groups was found to also significantly stabilize the *trans*-conformation ($\delta \approx 180$),[49] but intermolecular interactions with water molecules appear more likely than intramolecular contacts. Hence, we obtained seven stable conformers of **TA**, of which a

structure with two intramolecular hydrogen bonds was determined as the lowest energy conformer at the DFT level (Fig. 2 and Table 1).

As **TA** possesses four hydrogen bond donor groups and twelve acceptor sites, intermolecular interactions with polar solvent molecules cannot be neglected in the vibrational spectral calculations. In fact, in line with studies on **TA** in DMSO,[41] the spectra of **TA** in water cannot be simulated solely within a continuum solvation model (Fig. 3). Consequently, we considered a micro-solvation approach with up to four explicit water molecules directly bound to each hydrogen bond donor site of **TA**. Interestingly, while our study on proline showed that the relative spatial orientation of single water molecules can have a strong impact on the computed conformer spectra, the effect was little pronounced in the case of **TA** and limited to the vibrational modes directly associated with water (Fig. S2). Yet, the spectra of the three-fold solvated structures clearly did not match with the experimental band shapes, and the IR and VCD spectra of the four-fold solvated state also matched only for a few bands, such as the out-of-phase and in-phase couplet C-O stretching vibrations at 1140 and 1090 cm^{-1}, respectively (Fig. 3). It can thus be concluded that a micro-solvation approach, which considers only a small number of solvent water molecules, is not sufficient to reproduce all spectral features.

To better reproduce the spectrum of **TA** in water, we thus followed the solvent-shell approach that we already successfully applied to proline. It involves the simultaneous sampling of the solute and solvent conformational space by means of MD simulations. From independent trajectories, hundreds of solute–solvent configurations are extracted, which are reduced to smaller clusters **TA**–(H₂O)$_n$ that serve as a basis for DFT-based geometry optimizations and spectral calculations. In this study, we based the spectral analysis on QM/MM MD simulations, which described the solute **TA** at the semi-empirical level (AM1 and PM6) and the surrounding 530–550 water molecules with the TIP3P force field. Independent MD simulations of 30 ns were started from four different conformers of **TA**.

To first characterize the average size of the solvation shell around **TA** and to determine the number of solvent molecules to be considered in the subsequent DFT optimizations, the trajectories were evaluated regarding intra- and intermolecular hydrogen bonds. At both semi-empirical levels, there were typically no intramolecular hydrogen bonds and on average five direct solute–solvent interactions. For the first and second
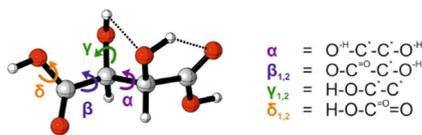

Fig. 2 Lowest energy conformer of **TA** at the B3LYP(G)/def2TZVP/CPCM(water) level of theory indicating the torsional angle definitions used throughout this work.

Table 1 Conformers of **TA** computed at the B3LYP(G)/def2TZVP/CPCM(water) level of theory. The torsional angles α, $\beta_{1/2}$ and $\gamma_{1/2}$ are defined in Fig. 2 and given in degrees. The relative zero-point corrected energies ΔE_{ZPC} are given in kcal mol^{-1}

Conf	α	β_1	β_2	γ_1	γ_2	ΔE_{ZPC}
C1	61.0	−1.3	172.8	−55.7	−121.0	0.00
C2	−159.3	−17.0	−17.0	−101.3	−101.3	1.83
C3	63.8	−178.9	−178.9	169.4	169.4	2.24
C4	−61.5	−29.5	−29.5	−83.9	−83.9	2.34
C5	−51.7	−23.1	−40.7	47.8	−88.9	2.43
C6	−71.1	151.4	−23.4	165.3	160.0	4.86
C7	−147.4	−158.7	−158.7	177.5	177.5	4.95

This journal is © the Owner Societies 2026

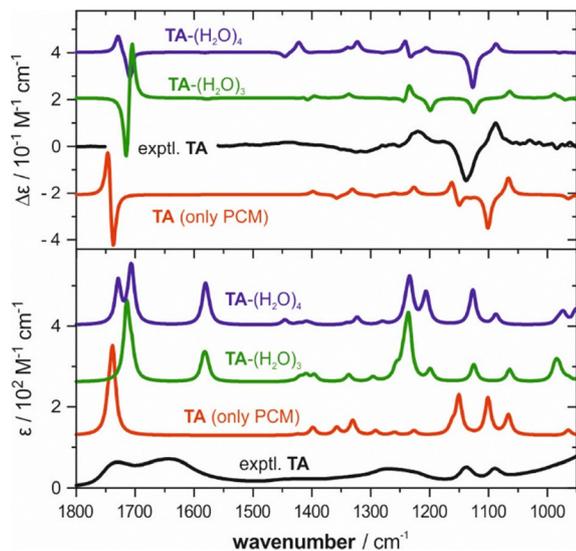*Phys. Chem. Chem. Phys.*, 2026, **28**, 1111–1117 | 1113

Fig. 3 Comparison of the experimental spectra of **TA** (pH = 1.5) with computed spectra obtained only in the PCM for water and by considering solute–solvent clusters **TA**–$(H_2O)_n$ with n = 3 and 4.

solvent shells, which are defined as all water molecules within the radius of 3.4 and 5 Å around **TA**, we obtained distributions centred around 16 and 55 water molecules. For our solvent-shell approach, we selected the cluster size to contain water molecules of ~1.5 solvent-shells, *i.e.*, we reduced the snapshots from the MD trajectories to **TA**–$(H_2O)_{30}$ clusters. Notably, although the conformer energies and structures of isolated **TA** predicted by AM1 and PM6 were quite different (Table S1), the conformational distributions obtained from the MD simulations were very similar (*cf.* Fig. 4 for AM1 and Fig. S3 for PM6). Likewise, after DFT optimization at the B3LYP(G)/def2TZVP/
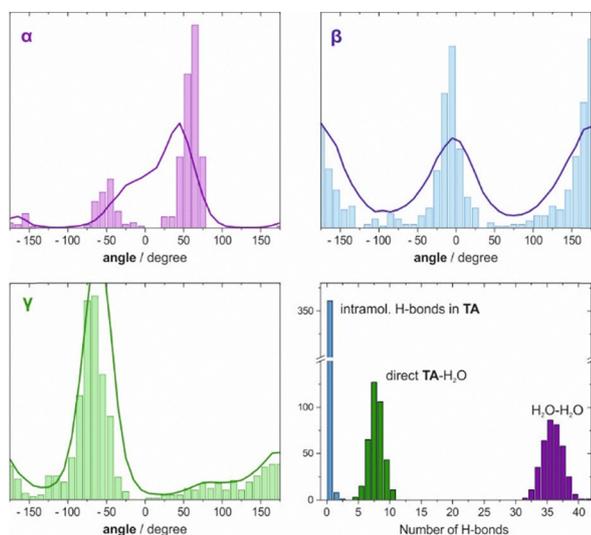
CPCM(water) level of theory, the conformational preferences of **TA** did not significantly change compared to the QM/MM-based distributions obtained from the MD, suggesting that the water environment also efficiently stabilizes non-equilibrium conformations. Solely, the average number of intermolecular hydrogen bonds slightly increased, probably due to differences in the cut-off definitions and small rearrangements within the water shell.

To obtain the VCD and IR spectra, the individual spectra of each of the approximately 400 optimized **TA**–$(H_2O)_{30}$ structures were simulated at a half-width at half-height of 6 cm^{-1} before calculating the plain average over all spectra (Fig. S4). Interestingly, in line with the very similar conformational preferences predicted by AM1 and PM6, the resulting spectra were basically identical (Fig. 5). Compared to the spectra of the smaller clusters (Fig. 3), the simulated spectra of **TA**–$(H_2O)_{30}$ matched nicely with the experimental band shapes, and even the line broadening was reproduced quite well. Being overcritical, it may be noted that the PM6-based spectra exhibit a marginally stronger negative signal in the range of 1400–1300 cm^{-1}, which slightly better reproduce the experimental result than AM1. However, the AM1-based spectra may be considered to match slightly better in the range of 1150–1050 cm^{-1}.

It is important to stress that the plain average over the hundreds of optimized snapshots provides a significantly better match with the experimental spectra than Boltzmann averaging over the optimized **TA**–$(H_2O)_{30}$ structures (Fig. S5). The relative energies of the cluster configurations are determined by the structure of the hydrogen bonding network, so that the latter approach puts weight on those few structures with the most favourable solvent–solvent interactions and the least dangling O–H groups. In the present case, a single structure out of all 400 optimized clusters carries a Boltzmann weight of >90%. This obviously misses the point of averaging solvent configurations.
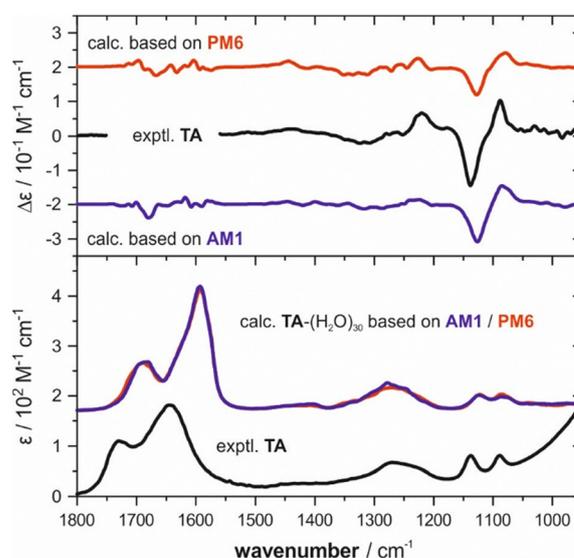

Fig. 4 Histograms showing the torsional angle distributions extracted from QM/MM-MD trajectories at the AM1 level (solid lines) and within the set of 400 optimized conformers **TA**–$(H_2O)_{30}$ (bars). For the optimized clusters, the number of intramolecular, intermolecular **TA**–H_2O and H_2O–H_2O hydrogen bonds is also counted.

Fig. 5 Comparison of the experimental VCD and IR spectra of **TA** with the computed spectra obtained by averaging **TA**–$(H_2O)_{30}$ clusters extracted from MD simulations at the AM1/TIP3P and PM6/TIP3P level of theory.
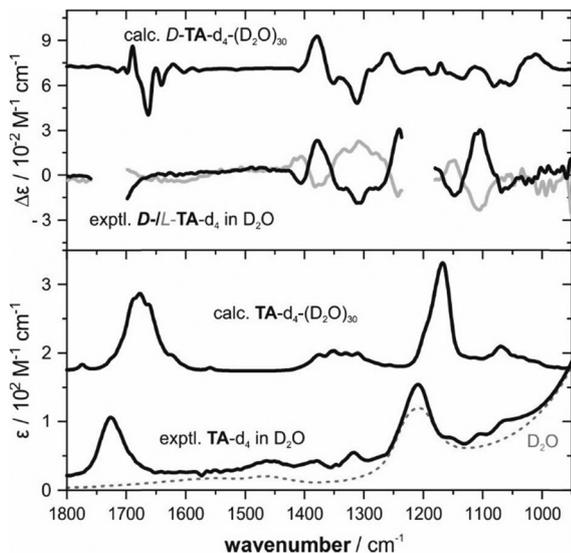
1114 | *Phys. Chem. Chem. Phys.*, 2026, **28**, 1111–1117

This journal is © the Owner Societies 2026

Fig. 6 Comparison of the experimental VCD and IR spectra of **TA** in D_2O with the computed spectra obtained by averaging **TA**-d_4–$(D_2O)_{30}$ clusters extracted from MD simulations at the AM1/TIP3P level of theory.

To further validate the solvent-shell approach for **TA**, we recorded the VCD and IR spectra of **TA** in D_2O (Fig. 6). Overall, the VCD band intensities were found to be lower than those in H_2O and, due to strong IR absorbance, the VCD spectrum could not be recorded in the range of the CO stretching vibration and within the range of the D_2O bending modes (1240–1180 cm^{-1}). Nonetheless, good mirror image quality was obtained which allowed for a detailed comparison with computed spectra. To account for the H/D-exchange in the calculations, we re-computed the vibrational spectra of **TA**-d_4–$(D_2O)_{30}$ based on the already optimized cluster geometries. The averaged VCD and IR spectra were found to provide a very good match with the experimental spectra, and it is particularly noteworthy that most of the details in the experimental VCD band shape are accurately reproduced.

Deprotonated tartaric acid: TA^{2-}–$(H_2O)_{30}$

In light of the exceptionally good match between the experimental spectra of neutral **TA** and the **TA**–$(H_2O)_{30}$ clusters, we did not attempt to compute spectra of **TA**$^{2-}$ with few water molecules but directly followed the solvent-shell approach. Three independent MD simulations were run for about 30 ns starting from different conformations. In contrast to the simulations on the neutral species, however, the resulting conformational distributions were significantly different for the two semi-empirical levels of theory (Fig. 7). While the carboxylate groups were obviously allowed to rotate freely (angle β), the central C–C bond is predicted to prefer a *gauche*(+) conformation (angle α, *i.e.*, a stretched carbon chain) by AM1, while it should adopt a *trans*-conformation according to the PM6 simulation. Consequently, the orientation of the O-H groups (angle γ) also differs between the distributions. Interestingly, already on the level of the dianionic species **TA**$^{2-}$ alone (Table S2), PM6 gives clearly difference preferences than AM1 or DFT.
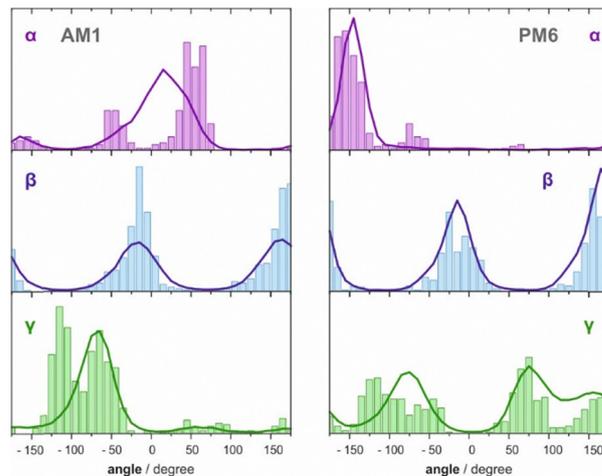

Fig. 7 Histograms showing the torsional angle distributions extracted from QM/MM-MD trajectories at the AM1 and PM6 levels (solid lines) compared to optimized conformers **TA**$^{2-}$–$(H_2O)_{30}$ (bars).

On the basis of about 330 structures of **TA**$^{2-}$–$(H_2O)_{30}$ extracted from the MD trajectories and optimized at the DFT level, we simulated the VCD and IR spectra for the two conformational distributions (Fig. 8). As expected, the comparison of the computed spectra directly revealed significant differences. The most pronounced example is the couplet of the C–O stretching modes in the range of 1150–1050 cm^{-1} which was only correctly reproduced based on the AM1 conformational preferences, while it inverted in sign according to the PM6 distribution. This sign inversion is an apparent consequence of the different conformational distributions, as the different preferences in the torsional angle α between the C–O bonds directly affect the coupling of the two oscillators.
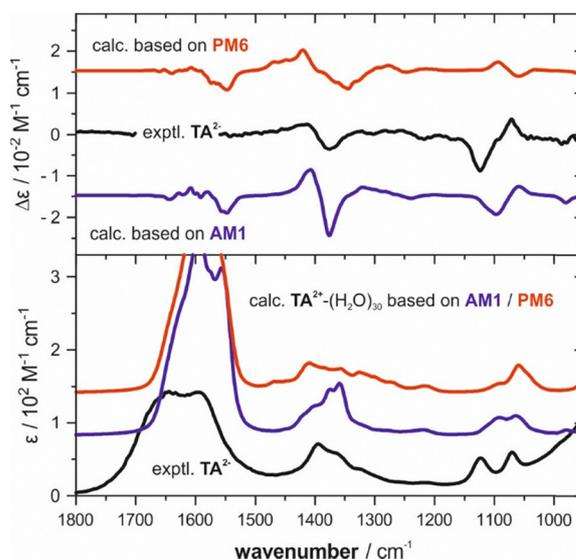

Fig. 8 Comparison of the experimental VCD and IR spectra of **TA**$^{2-}$ with the computed spectra obtained by averaging **TA**$^{2-}$–$(H_2O)_{30}$ clusters extracted from MD simulations at the AM1/TIP3P and PM6/TIP3P levels of theory.

Conclusions and outlook

In this work, we investigated the VCD and IR spectra of **TA** in aqueous solution. The experimental spectra of neutral **TA** and dianionic $\mathbf{TA^{2-}}$ were found to show distinct differences in their band shapes. For **TA** in H_2O, we demonstrated that a microsolvation approach with explicit consideration of three or four water molecules does not reproduce the full spectral band shapes. A solvent-shell approach that considered hundreds of solvation shell configurations in **TA**–$(H_2O)_{30}$ clusters extracted from QM/MM MD simulations demonstrated a very good agreement over the entire experimentally observed range for **TA** in both H_2O and, when re-computed as **TA**-d_4–$(D_2O)_{30}$, D_2O. Unlike for the neutral case, QM/MM MD simulations at the AM1 and PM6 levels gave significantly different conformational distributions for $\mathbf{TA^{2-}}$ in H_2O. Comparison of the computed spectra of $\mathbf{TA^{2-}}$–$(H_2O)_{30}$ with the experimental data confirmed that the AM1-based distribution provided a notably better agreement with the experiment, suggesting that the underlying conformational distribution more closely resembles the experimental system.

The observations described in this study further underline the need to consider more than a few water molecules when simulating VCD spectra for aqueous solutions. It has been demonstrated that reliable spectral calculations can be carried out using QM/MM MD simulations. Yet, as the number of considered structures must be sufficiently high to capture both the conformational distribution of the solute and the dynamics of the solvent shell, this approach will likely reach its limits for large and conformationally flexible molecules. Hence, future work should further explore these limits and approaches to effectively narrow down the number of structures to be computed.

Conflicts of interest

There are no conflicts to declare.

Data availability

The data supporting this article have been included as part of the supplementary information (SI). Supplementary information: Structures and energies of computed conformers, additional spectral plots, and analysis of MD simulations. See DOI: https://doi.org/10.1039/d5cp03705k.

Acknowledgements

References

1 L. A. Nafie, *Vibrational Optical Actvity*, John Wiley & Sons Ltd, UK, 2011.

2 P. J. Stephens, F. J. Devlin and J. R. Cheeseman, *VCD Spectroscopy for Organic Chemists*, CRC Press, 2012.

3 J. M. Batista Jr, E. W. Blanch and V. da Silva Bolzani, *Nat. Prod. Rep.*, 2015, **32**, 1280–1302.

4 C. Merten, T. P. Golub and N. M. Kreienborg, *J. Org. Chem.*, 2019, **84**, 8797–8814.

5 P. L. Polavarapu and E. Santoro, *Nat. Prod. Rep.*, 2020, **37**, 1661–1699.

6 C. Merten, *Phys. Chem. Chem. Phys.*, 2017, **19**, 18803–18812.

7 A. Bouchet, T. Brotin, M. Linares, H. Agren, D. Cavagnat and T. Buffeteau, *J. Org. Chem.*, 2011, **76**, 1372–1383.

8 L. Weirich and C. Merten, *Phys. Chem. Chem. Phys.*, 2021, **23**, 18300–18307.

9 L. Weirich, G. Tusha, E. Engelage, L. V. Schäfer and C. Merten, *Phys. Chem. Chem. Phys.*, 2022, **24**, 11721–11728.

10 C. Bravin, G. Mazzeo, S. Abbate, G. Licini, G. Longhi and C. Zonta, *Chem. Commun.*, 2022, **58**, 2152–2155.

11 M. A. J. Koenis, C. S. Chibueze, M. A. Jinks, V. P. Nicu, L. Visscher, S. M. Goldup and W. J. Buma, *Chem. Sci.*, 2020, **11**, 8469–8475.

12 V. Raghavan and P. L. Polavarapu, *Chirality*, 2017, **29**, 836–846.

13 S. Abbate, M. Passarello, F. Lebon, G. Longhi, A. Ruggirello, V. Turco Liveri, F. Viani, F. Castiglione, D. Mendola and A. Mele, *Chirality*, 2014, **26**, 532–538.

14 S. Abbate, R. Gangemi, F. Lebon, G. Longhi, M. Passarello, A. Ruggirello and V. Turco Liveri, *Vib. Spectrosc.*, 2012, **60**, 54–62.

15 S. Abbate, G. Longhi, A. Ruggirello and V. T. Liveri, *Colloids Surf., A*, 2008, **327**, 44–50.

16 C. Merten, C. H. Pollok, S. Liao and B. List, *Angew. Chem., Int. Ed.*, 2015, **54**, 8841–8845.

17 N. M. Kreienborg and C. Merten, *Chem. – Eur. J.*, 2018, **24**, 17948–17954.

18 C. Merten, *Eur. J. Org. Chem.*, 2020, 5892–5900.

19 T. P. Golub, A. H. Abazid, B. J. Nachtsheim and C. Merten, *Angew. Chem., Int. Ed.*, 2022, **61**, e202204624.

20 T. P. Golub, M. Feßner, E. Engelage and C. Merten, *Chem. – Eur. J.*, 2022, **28**, e202201317.

21 K. Bünnemann and C. Merten, *Phys. Chem. Chem. Phys.*, 2017, **19**, 18948–18956.

22 L. Weirich, J. Magalhaes de Oliveira and C. Merten, *Phys. Chem. Chem. Phys.*, 2020, **22**, 1525–1533.

23 C. Merten, *Phys. Chem. Chem. Phys.*, 2023, **25**, 29404–29414.

24 K. Le Barbu-Debus, J. Bowles, S. Jähnigen, C. Clavaguéra, F. Calvo, R. Vuilleumier and A. Zehnacker, *Phys. Chem. Chem. Phys.*, 2020, **22**, 26047–26068.

25 S. Jähnigen, D. Sebastiani and R. Vuilleumier, *Phys. Chem. Chem. Phys.*, 2021, **23**, 17232–17241.

26 A. S. Perera, J. Thomas, M. R. Poopari and Y. Xu, *Front Chem*, 2016, **4**, 9.

27 Y. Yang, M. Alshalalfeh and Y. Xu, *Spectrochim. Acta A*, 2024, **307**, 123634.

28 E. Y. Lee, V. M. S. Sousa, E. R. Mestriner, K. Bernardino, I. R. Nascimento and J. M. Batista, *Phys. Chem. Chem. Phys.*, 2025, **27**, 3908–3915.

1116 | *Phys. Chem. Chem. Phys.*, 2026, **28**, 1111–1117

This journal is © the Owner Societies 2026

29 T. A. Keiderling and A. Lakhani, *Comprehensive Chiroptical Spectroscopy*, John Wiley & Sons, Inc., 2012, pp. 707–758, DOI: **10.1002/9781118120392.ch22**.

30 T. A. Keiderling, *Chem. Rev.*, 2020, **120**, 3381–3419.

31 Z. Su, Q. Wen and Y. Xu, *J. Am. Chem. Soc.*, 2006, **128**, 6755.

32 A. S. Perera, C. D. Carlson, J. Cheramy and Y. Xu, *Chirality*, 2023, **35**, 718–731.

33 P. Fagan, L. Kocourkova, M. Tatarkovic, F. Kralik, M. Kuchar, V. Setnicka and P. Bour, *Chem. Phys. Chem.*, 2017, **18**, 2258–2265.

34 K. Dobšíková, P. Michal, D. Spálovská, M. Kuchař, N. Paškanová, R. Jurok, J. Kapitán and V. Setnička, *Analyst*, 2023, **148**, 1337–1348.

35 D. A. Drost and C. Merten, *Phys. Chem. Chem. Phys.*, 2024, **26**, 17753–17759.

36 H. Sugeta, C. Marcott, T. R. Faulkner, J. Overend and A. Moscowitz, *Chem. Phys. Lett.*, 1976, **40**, 397–398.

37 T. A. Keiderling and P. J. Stephens, *J. Am. Chem. Soc.*, 1977, **99**, 8061–8062.

38 C. N. Su and T. A. Keiderling, *J. Am. Chem. Soc.*, 1980, **102**, 511–515.

39 P. L. Polavarapu, C. S. Ewig and T. Chandramouly, *J. Am. Chem. Soc.*, 1987, **109**, 7382–7386.

40 A. Brizard, D. Berthier, C. Aimé, T. Buffeteau, D. Cavagnat, L. Ducasse, I. Huc and R. Oda, *Chirality*, 2009, **21**, E153–E162.

41 A. R. Puente and P. L. Polavarapu, *Spectrochim. Acta A*, 2023, **303**, 123231.

42 L. D. Barron, A. R. Gargaro, L. Hecht, P. L. Polavarapu and H. Sugeta, *Spectrochim. Acta A*, 1992, **48**, 1051–1066.

43 D. A. Case, H. M. Aktulga, K. Belfon, I. Y. Ben-Shalom, J. T. Berryman, S. R. Brozell, D. S. Cerutti, I. T. E. Cheatham, G. A. Cisneros, V. W. D. Cruzeiro, T. A. Darden, R. E. Duke, G. Giambasu, M. K. Gilson, H. Gohlke, A. W. Goetz, R. Harris, S. Izadi, S. A. Izmailov, K. Kasavajhala, M. C. Kaymak, E. King, A. Kovalenko, T. Kurtzman, T. S. Lee, S. LeGrand, P. Li, C. Lin, J. Liu, T. Luchko, R. Luo, M. Machado, V. Man, M. Manathunga, K. M. Merz, Y. Miao, O. Mikhailovskii, G. Monard, H. Nguyen, K. A. O'Hearn, A. Onufriev, F. Pan, S. Pantano, R. Qi, A. Rahnamoun, D. R. Roe, A. Roitberg, C. Sagui, S. Schott-Verdugo, A. Shajan, J. Shen, C. L. Simmerling, N. R. Skrynnikov, J. Smith, J. Swails, R. C. Walker, J. Wang, J. Wang, H. Wei, R. M. Wolf, X. Wu, Y. Xiong, Y. Xue, D. M. York, D. Zhao and P. A. Kollman, *Amber 2022*, University of California, San Francisco, 2022.

44 F. Neese, *WIREs Comput. Mol. Sci.*, 2012, **2**, 73–78.

45 F. Neese, F. Wennmohs, U. Becker and C. Riplinger, *J. Chem. Phys.*, 2020, **152**, 224108.

46 F. Neese, *WIREs Comput. Mol. Sci.*, 2022, **12**, e1606.

47 P. Comuzzo and F. Battistutta, in *Red Wine Technology*, ed. A. Morata, Academic Press, 2019, pp. 17–34, DOI: **10.1016/B978-0-12-814399-5.00002-5**.

48 K. Bünnemann, C. H. Pollok and C. Merten, *J. Phys. Chem. B*, 2018, **122**, 8056–8064.

49 E. R. Alonso, I. León, L. Kolesniková, S. Mata and J. L. Alonso, *Angew. Chem., Int. Ed.*, 2021, **60**, 17410–17414.

This journal is © the Owner Societies 2026

Phys. Chem. Chem. Phys., 2026, **28**, 1111–1117 | 1117